Letter

Absence of spin liquid phase in the $J_1 - J_2$ Heisenberg model on the square lattice

Xiangjian Qian [1] and Mingpu Qin [1,2,*]

[1] *Key Laboratory of Artificial Structures and Quantum Control (Ministry of Education), School of Physics and Astronomy, Shanghai Jiao Tong University, Shanghai 200240, China*

[2] *Hefei National Laboratory, Hefei 230088, China*

(Received 19 October 2023; revised 14 March 2024; accepted 18 March 2024; published 3 April 2024)

We perform an in-depth investigation of the phase diagram of the $J_1 - J_2$ Heisenberg model on the square lattice. We take advantage of density matrix renormalization group and fully augmented matrix product states methods and reach unprecedented accuracy with large bond dimensions. We utilize excited-level crossing analysis to pinpoint the phase transition points. It was believed before that there exists a narrow spin liquid phase sandwiched by the Néel antiferromagnetic (AFM) and valence bond solid (VBS) phases. Through careful finite-size scaling of the level crossing points, we find a direct phase transition between the Néel AFM and VBS phases at $J_2/J_1 = 0.535(3)$, suggesting the absence of an intermediate spin liquid phase. We also provide accurate results for ground-state energies for a variety of sizes, from which we find that the transition between the Néel AFM and VBS phases is continuous. These results indicate the existence of a deconfined quantum critical point at $J_2/J_1 = 0.535(3)$ in the model. From the crossing of the first derivative of the energies with J_2 for different sizes, we also determine the precise location of the first-order phase transition between the VBS and stripe AFM phases at $J_2/J_1 = 0.610(5)$.

DOI: 10.1103/PhysRevB.109.L161103

Introduction. The exploration of quantum phases and phase transitions in strongly correlated systems has long captivated the attention of physicists [1–3]. Such investigations provide crucial insights not only into the fundamental behavior of matter, but also into the exotic phenomena exhibited by these systems [4–15]. The $J_1 - J_2$ Heisenberg model on the square lattice is a prominent example. The Hamiltonian of the model is

$$H = J_1 \sum_{\langle i,j \rangle} S_i \cdot S_j + J_2 \sum_{\langle\langle i,j \rangle\rangle} S_i \cdot S_j, \tag{1}$$

where S_i is the spin-1/2 operator on site i, and the summations are taken over nearest-neighbor ($\langle i, j \rangle$) and next-nearest-neighbor ($\langle\langle i, k \rangle\rangle$) pairs, as shown in Fig. 1(a). This model, which comprises nearest-neighboring (J_1, the energy unit in this work) and next-nearest-neighboring (J_2) exchange interactions, exhibits a delicate interplay between competing magnetic interactions. This competition makes the model a well-known playground to search for exotic quantum states [quantum spin liquids (QSL), for example] other than on a geometrically frustrated lattice such as a kagome lattice [16–20]. The understanding of this kind of exotic states may serve as a critical piece in unraveling the enigmatic behavior of doped Mott materials and high-temperature superconductivity [21–27].

Over the past three decades, enormous research effort has been dedicated to the exploration of the phase diagram of the $J_1 - J_2$ Heisenberg model on the square lattice. This model has become a focal point in the study of quantum magnetism. It has become evident that distinct magnetic orders emerge at different regimes of the parameter space. In the zero J_2 limit, the ground state displaces Néel antiferromagnetic (AFM) order [28] which stretches to a finite J_2 value. In the opposite limit where J_2 is infinitely large, the model decouples into two isolated Heisenberg models on the two sublattices of the original square lattice. A large but finite J_2 couples these two sublattices and the ground state is known to have the so-called stripe AFM order [29,30]. In the intermediate range, roughly encompassing $0.5 \lesssim J_2 \lesssim 0.6$, an intriguing nonmagnetic regime emerges. These insights have been gleaned through a multifaceted approach, including exact diagonalizations [29,31–33], series expansions [34–36], density-matrix renormalization group (DMRG) [37–39], (infinite) projected entangled-pair state [(i)PEPS] [40–44], neural network [45], and quantum Monte Carlo (QMC) [30,46,47].

However, despite the wealth of results and analyses, the nature of the nonmagnetic regime in the $0.5 \lesssim J_2 \lesssim 0.6$ range remains a subject of intense debate and active research. Within this intriguing region, several competing states have been found with a variety of methods. These states include columnar valence bond solid (VBS) [35,48,49] and plaquette VBS [33,38,50,51], as well as quantum spin liquids with [37] or without [39,42,45,46] a spin gap.

Much of the controversy surrounding this topic can be attributed to the difficulty of simulating large systems with enough accuracy and the challenges posed by finite-size scaling of the order parameters or gaps, which could introduce large uncertainties near the critical points [52–56]. To address these issues, we adopt the level-spectroscopy approach, in which the finite-size transition points are determined through

*qinmingpu@sjtu.edu.cn

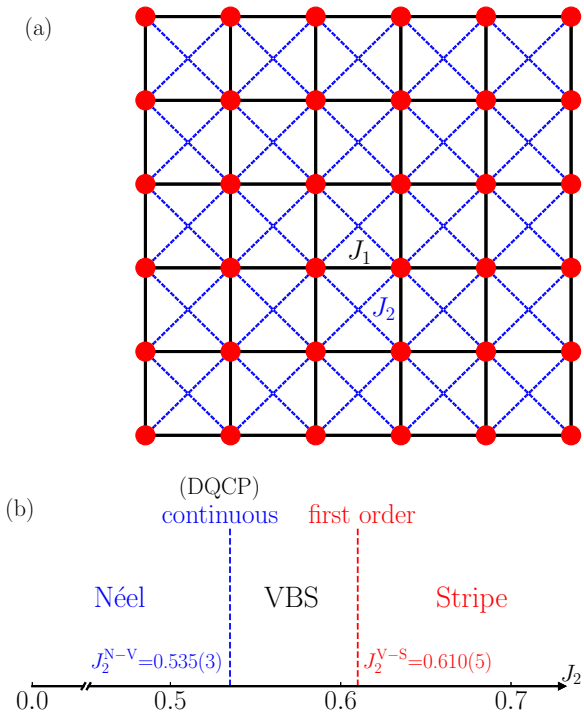

FIG. 1. (a) The illustration of the $J_1 - J_2$ Heisenberg model on the square lattice, with black and dashed blue lines indicating the nearest-neighboring interaction J_1 and next-nearest-neighboring interaction J_2, respectively. (b) The ground-state phase diagram of the $J_1 - J_2$ Heisenberg model on the square lattice with J_2 (we set $J_1 = 1$ as the energy unit). We find three different phases with the variation of J_2: Néel AFM, VBS, and stripe AFM. We find a direct continuous phase transition between the Néel AFM and VBS phases at $J_2^{\text{N-V}} = 0.535(3)$, ruling out the existence of a quantum spin liquid phase between them, indicating the existence of a deconfined quantum critical point between the Néel AFM and VBS phases. At $J_2^{\text{V-S}} = 0.610(5)$, a first-order transition occurs between the VBS and stripe AFM phases.

the identification of excited-level crossings [39,52,55–60]. This approach was widely adopted in very recent studies of the same model studied in this work and other models [39,45,61,62]. The smooth size dependence exhibited by these crossing points allows for more reliable extrapolations to the thermodynamic limit, surpassing the limitations encountered in past studies relying solely on order parameters, thus allowing us to accurately determine the phase boundaries.

In this Letter, we perform an in-depth investigation of the $J_1 - J_2$ Heisenberg model on the square lattice using state-of-the-art numerical techniques, including DMRG [63–65] and the recently developed Fully Augmented Matrix Product States (FAMPS) methods [66]. We take advantage of the SU(2) symmetry in the calculations and reach bond dimension (kept states) up to as large as 15 000 SU(2) multiplets, which contains about 60 000 U(1) states. For FAMPS [66], we preserve up to equivalently 22 000 U(1) states [67]. We obtain accurate results on cylinders with width up to 14 by careful extrapolations with truncation errors in both DMRG and FAMPS. By utilizing the level spectroscopy combined with reliable finite-size scaling, we find a direct phase transition between Néel AFM and VBS phases at $J_2^{\text{N-V}} = 0.535(3)$—in contrast to the previous predictions of a QSL phase between them. We observe no tendency of singularity in the first and second derivative of the ground-state energy with respect to J_2 at this transition point, indicating that the transition between the Néel AFM and VBS phases is continuous. This evidence implies that this transition is a deconfined quantum critical [7,8] type. The characterization of this transition deserves further investigation. We also determine the precise location of the first-order phase transition between the VBS and stripe phases at $J_2^{\text{V-S}} = 0.610(5)$ from the crossing of the first derivative of the energies with J_2 for different sizes. An illustration of the phase diagram is shown in Fig. 1(b).

Methods. DMRG is now arguably the workhorse for the accurate simulation of one-dimensional and quasi-one-dimensional quantum systems [63–65]. As a variational method, the wave-function ansatz of DMRG is known as matrix product states (MPS) [68–70], which is defined as

$$|\text{MPS}\rangle = \sum_{\{\sigma_i\}} \text{Tr}[A^{\sigma_1} A^{\sigma_2} A^{\sigma_3} \cdots A^{\sigma_n}] |\sigma_1 \sigma_2 \sigma_3 \cdots \sigma_n\rangle, \tag{2}$$

where A is a rank-3 tensor with one physical index σ_i with dimension d and two auxiliary indices with dimension D. DMRG has also been widely used in the study of two-dimensional quantum systems with narrow cylinder geometries [22,23,25–27].

In the pursuit of even higher accuracy and the alleviation of the entanglement limitation in the simulation of wider systems with DMRG, we resort to a recently developed method named FAMPS [66]. FAMPS is an extension of DMRG by adding an additional layer of tensors known as disentanglers [71] connecting to the physical indices of DMRG. It is defined as

$$|\text{FAMPS}\rangle = D(u)|\text{MPS}\rangle, \tag{3}$$

where $D(u) = \prod_m u_m$ denotes an additional disentangler layer. This extension empowers FAMPS with the extraordinary capability to produce more accurate results for wider quantum systems, while maintaining the computational efficiency [$O(D^3)$] [66,72,73] of DMRG with small overhead [$O(d^4)$].

Moreover, we have invested efforts into optimizing the code efficiency. Through techniques such as parallelization and the exploitation of SU(2) symmetry [74,75], we are able to push the kept states which determine the accuracy of the simulation in DMRG and FAMPS to an unprecedented value, i.e., 60 000 (22 000) U(1) states for DMRG (FAMPS), setting a higher limit of the numerical simulation.

We employ these state-of-the-art numerical techniques on a diverse set of $L \times 2L$ cylinder systems, spanning a range of sizes from $L = 6$ to $L = 14$ and J_2 values from $J_2 = 0.45$ to $J_2 = 0.65$, and giving well-converged results with extrapolation with truncation errors in DMRG and FAMPS calculations.

As mentioned earlier, we utilize the level crossing of excited states with different quantum numbers to determine the phase transition points. For excitations in the $S = 0$ sector, we target multiple states [64,76,77] in the $S = 0$ subspace since the ground state lies in the $S = 0$ sector. For excitations in the $S = 1$ and $S = 2$ sectors, we obtain the energies by

performing the calculation in the desired subspace to obtain the excited state.

Level spectroscopy. We begin our investigation by studying the region between the Néel AFM and the VBS phases. Historically, the regime encompassing $0.5 \lesssim J_2 \lesssim 0.6$ has been a focal point of considerable debate and intensive research. Numerous investigations, predominantly reliant on order parameters, have sought to elucidate the distinct phases characterizing this intricate region. Recent developments have resulted in a growing consensus that the emergence of the VBS state occurs within this region with onset J_2 varying from 0.52 to 0.56 [38,42,45,78]. However, a contentious issue lingers concerning the potential possibility of a QSL phase at smaller values of J_2 (approximately $J_2 \approx 0.5$) [38,40,41,43,45]. This controversy primarily arises from the finite-size scaling of order parameters or gaps, which could introduce large uncertainties near the critical points, thus challenging the precise determination of critical points and phase boundaries within this regime [55].

In Refs. [39,52,55–60], the authors introduced a numerical level-spectroscopy method, wherein finite-size transition points are identified through excited energy crossings. This approach is rooted in the fundamental understanding that quantum phases are distinguished by their distinctive characteristics within excitation spectra. In finite-size systems, low-lying excitations bear distinct quantum numbers corresponding to different phases, rendering them invaluable probes for the detection and characterization of phase transitions. This innovative approach is known to have a smooth finite-size scaling [55], allowing us to accurately determine the phase boundary. This method was also adopted in recent studies of the same model studied in this work [39,45]. Specifically, the crossing point between the singlet and quintuplet excited states, denoted as $J_2^{c_1}$, is interpreted as the Néel AFM phase boundary, and the crossing point between the singlet and triplet excited states, marked as $J_2^{c_2}$, is identified as the onset of the VBS phase [39].

In Ref. [39], the authors determined the phase diagram by DMRG with the level-spectroscopy method. However, due to the limited system sizes calculated in Ref. [39], it is not easy to determine the actual finite-size scaling behavior of the excited-level crossing points.

Our current study leverages the enhanced capabilities of both DMRG and advanced FAMPS algorithms, enabling us to accurately simulate systems with sizes up to $L = 14$ and perform more reliable analyses of the finite-size scaling behavior of the level-crossing points. Figure 2 presents the excited-level crossing points $J_2^{c_1}$ and $J_2^{c_2}$ as a function of $1/L$. The excited-level crossing points for $L \leqslant 10$ are consistent between the previous work [39] and our results. Remarkably, it is clear from the data that the crossing points scale as $1/L$ instead of the previously assumed $1/L^2$ [59,60]. In Fig. 2(b), we also show a plot of crossing points versus $1/L^2$ for the same data, which clearly deviates from a straight line.

Extrapolating the level-crossing points through linear fits yields $J_2^{c_1} = 0.537(4)$ and $J_2^{c_2} = 0.533(1)$, suggesting a direct transition between the Néel AFM and VBS phases, ruling out the presence of an intermediate QSL phase. We also perform the same linear fit of the level-crossing points for systems on torus accurately calculated by Nomura *et al.* in [45], which

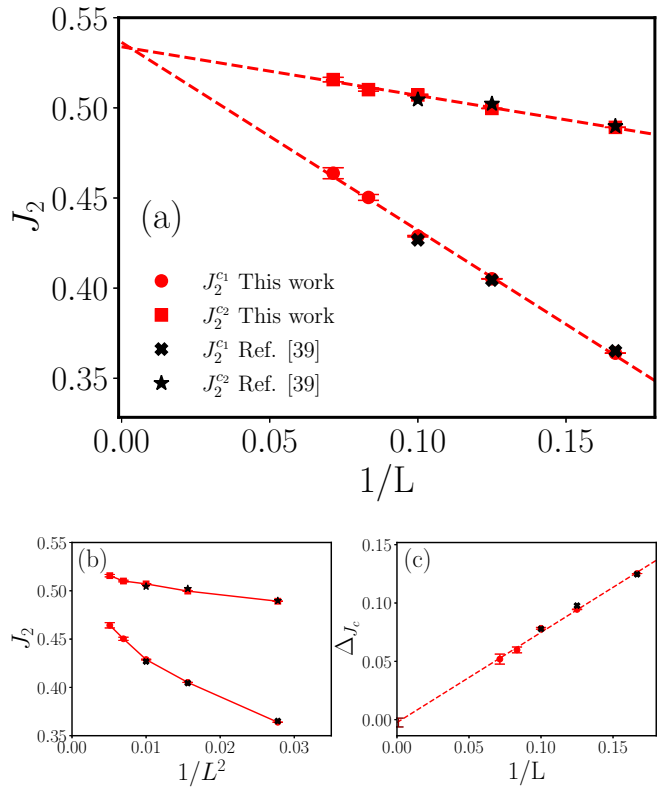

FIG. 2. (a) The excited-level crossing points $J_2^{c_1}$ and $J_2^{c_2}$ as a function of $1/L$. The singlet-quintuplet crossing point $J_2^{c_1}$ is interpreted as a Néel AFM phase boundary and the singlet-triplet crossing point $J_2^{c_2}$ is identified as the onset of a VBS phase [39]. We also include the results from Ref. [39], which are consistent with our results. The extrapolated critical points by linear fits are $J_2^{c_1} = 0.537(4)$, $J_2^{c_2} = 0.533(1)$, providing strong evidence in favor of a direct transition between the Néel AFM and VBS states, ruling out the presence of an intermediate QSL phase. (b) We plot the same data in (a) by changing the x axis to $1/L^2$. We can clearly see the deviation from a straight line of the data. (c) The difference of the two crossing points, $\Delta_{J_c} = J_2^{c_2} - J_2^{c_1}$, vs $1/L$. We can clearly see that Δ_{J_c} scales linearly with $1/L$ and vanishes in the thermodynamic limit.

gives $J_2^{c_1} = 0.5344(7)$ and $J_2^{c_2} = 0.538(2)$, consistent with our results.

Furthermore, we also show the difference of the two crossing points, $\Delta_{J_c} = J_2^{c_2} - J_2^{c_1}$, as a function of $1/L$ in Fig. 2(c) which goes to zero linearly with $1/L$, indicating the absence of an intermediate spin liquid phase.

In Fig. 3, we show how to determine the crossing points of excitation levels by taking the 10×20 cylinder system as an example. Results for other sizes can be found in the Supplemental Material [79]. In Fig. 3(a), we plot the energies for the singlet and quintuplet excitations for $J_2 = 0.42$ and 0.43. With the extrapolations of truncation errors, we obtain the accurate energies of the singlet and quintuplet excitations and the difference between them, as shown in Fig. 3(c). Then a linear interpolation gives the crossing point (i.e., the point where $E_2 - E_0 = 0$). Using a similar procedure, we determine the crossing point for singlet and triplet excitations, as depicted in Figs. 3(b) and 3(d).

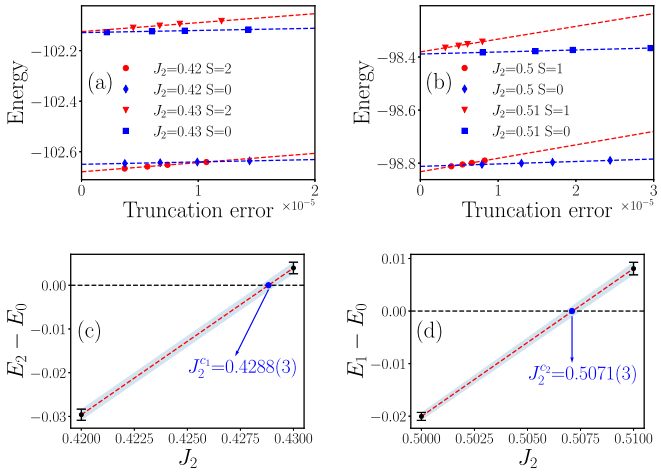

FIG. 3. Energies of the excitations in the $S = 0$, 1, and 2 sectors for a few J_2 values of a 10×20 cylinder system calculated by DMRG. In (a) and (b), DMRG energies are plotted as a function of truncation errors. We keep maximally equivalent 40 000 U(1) states in these DMRG calculations to ensure the convergence of the results. The excited state in the $S = 0$ sector is calculated with the multitarget states' DMRG algorithm [64,76,77]. (c), (d) The interpolation procedure to determine the excited-level crossing points for singlet-quintuplet and singlet-triplet excitations, respectively.

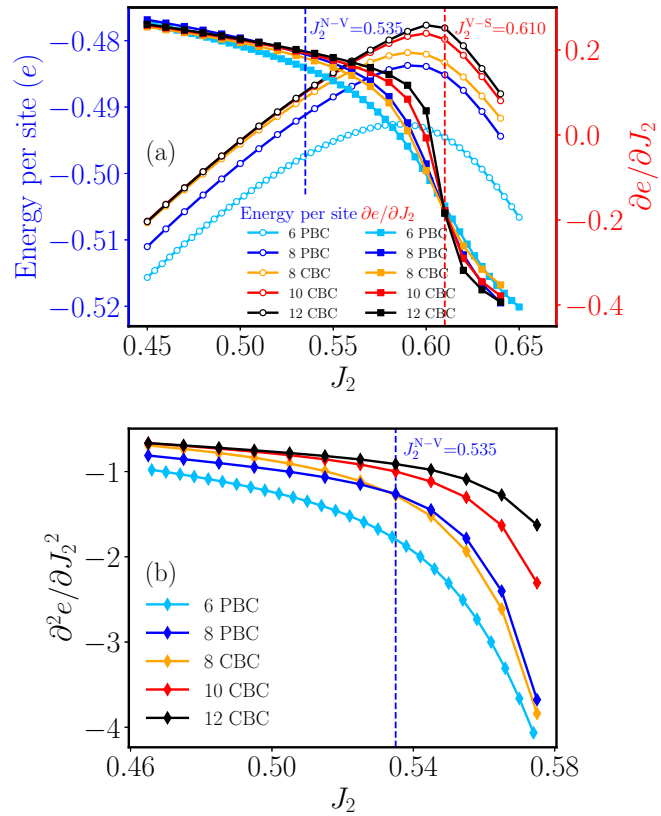

FIG. 4. (a) The ground-state energy per site e and its first derivative $\partial e/\partial J_2$ as a function of J_2 for $L \times L$ systems with periodic boundary conditions (PBCs) and $L \times 2L$ systems with cylinder boundary conditions (CBCs). Here, we find that the phase transition between Néel AFM and VBS phases at $J_2^{\text{N-V}} = 0.535$ is continuous. The crossing point of $\partial e/\partial J_2$ gives a precise location of the first-order transition between VBS and stripe AFM phases at $J_2^{\text{V-S}} = 0.610$ (see the text for more discussions). (b) The second derivative of the ground-state energy as a function of J_2 for different systems. The calculations are performed using DMRG, with a maximum of equivalent 60 000 U(1) states retained, except for 6×6 PBC systems which are calculated by exact diagonalization [80].

In the Supplemental Material [79], we calculate the staggered magnetization of the Néel AFM order at $J_2 = 0.5$, which is clearly nonzero (about 0.05). This result shows that $J_2 = 0.5$ is in the Néel AFM phase. The boundary of the Néel AFM phase obtained from the finite-size scaling of the crossing point of correlation length is $J_2 = 0.530$ (details can be found in the Supplemental Material [79]), consistent with the results from level-crossing analysis.

Energetics. We also study the behavior of ground-state energy versus J_2 to detect the quantum phase transitions. Figure 4(a) shows the ground-state energy density e and its first derivative $\partial e/\partial J_2$ as a function of J_2. We calculate $\partial e/\partial J_2$ from the expectation value of the J_2 term in the ground state according to the Feynman-Hellmann theorem. We show results for both torus systems (6×6 and 8×8) and cylinder systems (8×16, 10×20, and 12×24). Here we only show the results with the largest bond dimensions reached (the convergence of these results with bond dimensions can be found in the Supplemental Material [79]).

At the aforementioned critical point, $J_2^{\text{N-V}} = 0.535$, it is intriguing to note that $\partial e/\partial J_2$ is continuous. This behavior strongly suggests that the transition between the Néel AFM and the VBS phases is continuous. This observation aligns with the concept of deconfined quantum critical point (DQCP) [7,8], which is proposed to elucidate the continuous phase transition between the Néel AFM state and the VBS state. We notice that the deconfined criticality near $J_2 = 0.54$ was claimed before [38,40,43,45,78,81]. We also calculate the second derivative of the ground-state energy with respect to J_2, i.e., $\partial^2 e/\partial {J_2}^2$, using the finite-difference method, as shown in Fig. 4(b). Interestingly, there is no tendency of singularity at the critical point between the Néel AFM and the VBS phases near $J_2^{\text{N-V}} = 0.535$ in $\partial^2 e/\partial {J_2}^2$, suggesting that the phase transition is a high-order one. Further characterization of this phase transition requires additional investigations.

Finally, we shift our focus to the easier segment of the phase diagram. It was established that a first-order phase transition exists between the VBS and stripe AFM phases at $J_2 \approx 0.6$ [29,30]. In Fig. 4(a), we can clearly find a discontinuity in the $\partial e/\partial J_2$ plot near $J_2 = 0.6$. As elucidated in Ref. [82], for a first-order transition, finite-size scaling analysis reveals a distinct point denoted as $h(L)$. At this point $h(L)$, the quantity $M_{\text{per}}[h(L), L]$ remains constant with the varying of system size L. Furthermore, the difference between $h(L)$ and h_c is bounded by $O(e^{-L})$. Here, h represents the parameter driving the phase transition, h_c is the critical point at the thermodynamic limit, while M_{per} corresponds to either the order parameter or the first derivative of the free-energy density. The exponentially small difference between $h(L)$ and h_c suggests the existence of a fixed point for the first derivative of the free-energy density and allows us to accurately determine the location of the first-order transition. In Fig. 4(a), we

can clearly find a fixed point in $\partial e/\partial J_2$ at $J_2 = 0.610$. We thus conclude that the first-order transition between the VBS and stripe AFM phases occurs at $J_2 = 0.610(5)$.

Conclusions. With accurate DMRG and FAMPS results and careful finite-size scaling of the excited-level crossing points, we demonstrate a direct phase transition between the Néel AFM and the VBS phases at $J_2^{\text{N-V}} = 0.535(3)$ for the $J_1 - J_2$ Heisenberg model on the square lattice, indicating the absence of the previously claimed intermediate quantum spin liquid phases [37,39,42,45,46]. Moreover, the results from energy show that the phase transition is continuous, suggesting a deconfined quantum critical point at $J_2^{\text{N-V}} = 0.535(3)$, which deserves further explorations. We also determine the precise location of the first-order phase transition between the VBS and stripe phases at $J_2^{\text{V-S}} = 0.610(5)$ from the crossing of the first derivative of energy for different system sizes.

Looking ahead, the absence of a spin liquid phase in the $J_1 - J_2$ Heisenberg model on the square lattice prompts further inquiries into the roles of additional interactions and lattice geometries in shaping the behavior of quantum materials [16,17,19,78,81].

Acknowledgments. The calculation in this work is carried out with TensorKit [83]. The computation in this Letter were run on the Siyuan-1 cluster supported by the Center for High Performance Computing at Shanghai Jiao Tong University. M.Q. acknowledges the support from the National Key Research and Development Program of MOST of China (Grant No. 2022YFA1405400), the Innovation Program for Quantum Science and Technology (Grant No. 2021ZD0301902), the National Natural Science Foundation of China (Grant No. 12274290), and the sponsorship from Yangyang Development Fund.

[1] D. Cabra, A. Honecker, and P. Pujol, *Modern Theories of Many-Particle Systems in Condensed Matter Physics* (Springer, Berlin, 2012), Vol. 843.

[2] X. G. Wen, *Quantum Field Theory of Many-body Systems: From the Origin of Sound to an Origin of Light and Electrons* (Oxford University Press, Oxford, 2007).

[3] E. C. Marino, *Quantum Field Theory Approach to Condensed Matter Physics* (Cambridge University Press, Cambridge, 2017).

[4] Y. Cui, L. Liu, H. Lin, K.-H. Wu, W. Hong, X. Liu, C. Li, Z. Hu, N. Xi, S. Li, R. Yu, A. W. Sandvik, and W. Yu, Proximate deconfined quantum critical point in $SrCu_2(BO_3)_2$, Science **380**, 1179 (2023).

[5] L. Balents, Spin liquids in frustrated magnets, Nature (London) **464**, 199 (2010).

[6] L. Savary and L. Balents, Quantum spin liquids: A review, Rep. Prog. Phys. **80**, 016502 (2017).

[7] T. Senthil, A. Vishwanath, L. Balents, S. Sachdev, and M. P. A. Fisher, Deconfined quantum critical points, Science **303**, 1490 (2004).

[8] T. Senthil, Deconfined quantum critical points: A review, arXiv:2306.12638.

[9] F. Wilczek, Quantum mechanics of fractional-spin particles, Phys. Rev. Lett. **49**, 957 (1982).

[10] B. I. Halperin, Statistics of quasiparticles and the hierarchy of fractional quantized Hall states, Phys. Rev. Lett. **52**, 1583 (1984).

[11] D. Arovas, J. R. Schrieffer, and F. Wilczek, Fractional statistics and the quantum Hall effect, Phys. Rev. Lett. **53**, 722 (1984).

[12] C. Han, Z. Iftikhar, Y. Kleeorin, A. Anthore, F. Pierre, Y. Meir, A. K. Mitchell, and E. Sela, Fractional entropy of multichannel Kondo systems from conductance-charge relations, Phys. Rev. Lett. **128**, 146803 (2022).

[13] M. Brooks, M. Lemeshko, D. Lundholm, and E. Yakaboylu, Molecular impurities as a realization of anyons on the two-sphere, Phys. Rev. Lett. **126**, 015301 (2021).

[14] A. W. W. Ludwig, D. Poilblanc, S. Trebst, and M. Troyer, Two-dimensional quantum liquids from interacting non-Abelian anyons, New J. Phys. **13**, 045014 (2011).

[15] H. Nakano, Y. Minami, and S. I. Sasa, Long-range phase order in two dimensions under shear flow, Phys. Rev. Lett. **126**, 160604 (2021).

[16] S. Yan, D. A. Huse, and S. R. White, Spin-liquid ground state of the $S = 1/2$ kagome Heisenberg antiferromagnet, Science **332**, 1173 (2011).

[17] S. Depenbrock, I. P. McCulloch, and U. Schollwöck, Nature of the spin-liquid ground state of the $S = 1/2$ Heisenberg model on the kagome lattice, Phys. Rev. Lett. **109**, 067201 (2012).

[18] Y. Iqbal, F. Becca, S. Sorella, and D. Poilblanc, Gapless spin-liquid phase in the kagome spin-$\frac{1}{2}$ Heisenberg antiferromagnet, Phys. Rev. B **87**, 060405(R) (2013).

[19] H. J. Liao, Z. Y. Xie, J. Chen, Z. Y. Liu, H. D. Xie, R. Z. Huang, B. Normand, and T. Xiang, Gapless spin-liquid ground state in the $S = 1/2$ kagome antiferromagnet, Phys. Rev. Lett. **118**, 137202 (2017).

[20] Y.-C. He, M. P. Zaletel, M. Oshikawa, and F. Pollmann, Signatures of Dirac cones in a DMRG study of the kagome Heisenberg model, Phys. Rev. X **7**, 031020 (2017).

[21] P. A. Lee, N. Nagaosa, and X.-G. Wen, Doping a Mott insulator: Physics of high-temperature superconductivity, Rev. Mod. Phys. **78**, 17 (2006).

[22] H.-C. Jiang and S. A. Kivelson, High temperature superconductivity in a lightly doped quantum spin liquid, Phys. Rev. Lett. **127**, 097002 (2021).

[23] S. Jiang, D. J. Scalapino, and S. R. White, Ground-state phase diagram of the t-t'-J model, Proc. Natl. Acad. Sci. USA **118**, e2109978118 (2021).

[24] C.-M. Chung, M. Qin, S. Zhang, U. Schollwöck, and S. R. White (The Simons Collaboration on the Many-Electron Problem), Plaquette versus ordinary d-wave pairing in the t'-Hubbard model on a width-4 cylinder, Phys. Rev. B **102**, 041106(R) (2020).

[25] H. Xu, C.-M. Chung, M. Qin, U. Schollwöck, S. R. White, and S. Zhang, Coexistence of superconductivity with partially filled stripes in the Hubbard model, arXiv:2303.08376.

[26] X. Lu, J.-X. Zhang, S.-S. Gong, D. N. Sheng, and Z.-Y. Weng, Sign structure in the square-lattice t-t'-J model and numerical consequences, arXiv:2303.13498.

[27] D.-W. Qu, B.-B. Chen, X. Lu, Q. Li, Y. Qi, S.-S. Gong, W. Li, and G. Su, d-wave superconductivity, pseudogap, and the phase diagram of t-t'-J model at finite temperature, arXiv:2211.06322.

[28] A. W. Sandvik, Finite-size scaling of the ground-state parameters of the two-dimensional Heisenberg model, Phys. Rev. B **56**, 11678 (1997).

[29] E. Dagotto and A. Moreo, Phase diagram of the frustrated spin-1/2 Heisenberg antiferromagnet in 2 dimensions, Phys. Rev. Lett. **63**, 2148 (1989).

[30] S. Morita, R. Kaneko, and M. Imada, Quantum spin liquid in spin 1/2 J_1-J_2 Heisenberg model on square lattice: Many-variable variational Monte Carlo study combined with quantum-number projections, J. Phys. Soc. Jpn. **84**, 024720 (2015).

[31] D. Poilblanc, E. Gagliano, S. Bacci, and E. Dagotto, Static and dynamical correlations in a spin-1/2 frustrated antiferromagnet, Phys. Rev. B **43**, 10970 (1991).

[32] H. J. Schulz, T. A. L. Ziman, and D. Poilblanc, Magnetic order and disorder in the frustrated quantum Heisenberg antiferromagnet in two dimensions, J. Phys. I (France) **6**, 675 (1996).

[33] M. Mambrini, A. Läuchli, D. Poilblanc, and F. Mila, Plaquette valence-bond crystal in the frustrated Heisenberg quantum antiferromagnet on the square lattice, Phys. Rev. B **74**, 144422 (2006).

[34] J. Oitmaa and Zheng Weihong, Series expansion for the J_1-J_2 Heisenberg antiferromagnet on a square lattice, Phys. Rev. B **54**, 3022 (1996).

[35] R. R. P. Singh, Z. Weihong, C. J. Hamer, and J. Oitmaa, Dimer order with striped correlations in the J_1-J_2 Heisenberg model, Phys. Rev. B **60**, 7278 (1999).

[36] J. Sirker, Z. Weihong, O. P. Sushkov, and J. Oitmaa, J_1-J_2 model: First-order phase transition versus deconfinement of spinons, Phys. Rev. B **73**, 184420 (2006).

[37] H.-C. Jiang, H. Yao, and L. Balents, Spin liquid ground state of the spin-$\frac{1}{2}$ square J_1-J_2 Heisenberg model, Phys. Rev. B **86**, 024424 (2012).

[38] S.-S. Gong, W. Zhu, D. N. Sheng, O. I. Motrunich, and M. P. A. Fisher, Plaquette ordered phase and quantum phase diagram in the spin-$\frac{1}{2}J_1-J_2$ square Heisenberg model, Phys. Rev. Lett. **113**, 027201 (2014).

[39] L. Wang and A. W. Sandvik, Critical level crossings and gapless spin liquid in the square-lattice spin-$1/2J_1-J_2$ Heisenberg antiferromagnet, Phys. Rev. Lett. **121**, 107202 (2018).

[40] R. Haghshenas and D. N. Sheng, U(1)-symmetric infinite projected entangled-pair states study of the spin-1/2 square J_1-J_2 Heisenberg model, Phys. Rev. B **97**, 174408 (2018).

[41] J. Hasik, D. Poilblanc, and F. Becca, Investigation of the Néel phase of the frustrated Heisenberg antiferromagnet by differentiable symmetric tensor networks, SciPost Phys. **10**, 012 (2021).

[42] W.-Y. Liu, S.-S. Gong, Y.-B. Li, D. Poilblanc, W.-Q. Chen, and Z.-C. Gu, Gapless quantum spin liquid and global phase diagram of the spin-1/2 J_1-J_2 square antiferromagnetic Heisenberg model, Sci. Bull. **67**, 1034 (2022).

[43] L. Wang, Z.-C. Gu, F. Verstraete, and X.-G. Wen, Tensor-product state approach to spin-$\frac{1}{2}$ square J_1-J_2 antiferromagnetic Heisenberg model: Evidence for deconfined quantum criticality, Phys. Rev. B **94**, 075143 (2016).

[44] L. Vanderstraeten, L. Burgelman, B. Ponsioen, M. Van Damme, B. Vanhecke, P. Corboz, J. Haegeman, and F. Verstraete, Variational methods for contracting projected entangled-pair states, Phys. Rev. B **105**, 195140 (2022).

[45] Y. Nomura and M. Imada, Dirac-type nodal spin liquid revealed by refined quantum many-body solver using neural-network wave function, correlation ratio, and level spectroscopy, Phys. Rev. X **11**, 031034 (2021).

[46] W.-J. Hu, F. Becca, A. Parola, and S. Sorella, Direct evidence for a gapless Z_2 spin liquid by frustrating néel antiferromagnetism, Phys. Rev. B **88**, 060402(R) (2013).

[47] F. Ferrari and F. Becca, Gapless spin liquid and valence-bond solid in the J_1-J_2 Heisenberg model on the square lattice: Insights from singlet and triplet excitations, Phys. Rev. B **102**, 014417 (2020).

[48] R. R. P. Singh and R. Narayanan, Dimer versus twist order in the J_1-J_2 model, Phys. Rev. Lett. **65**, 1072 (1990).

[49] N. Read and S. Sachdev, Large-N expansion for frustrated quantum antiferromagnets, Phys. Rev. Lett. **66**, 1773 (1991).

[50] L. Capriotti and S. Sorella, Spontaneous plaquette dimerization in the J_1-J_2 Heisenberg model, Phys. Rev. Lett. **84**, 3173 (2000).

[51] J.-F. Yu and Y.-J. Kao, Spin-$\frac{1}{2}J_1$-J_2 Heisenberg antiferromagnet on a square lattice: A plaquette renormalized tensor network study, Phys. Rev. B **85**, 094407 (2012).

[52] K. Nomura, Correlation functions of the 2D sine-Gordon model, J. Phys. A: Math. Gen. **28**, 5451 (1995).

[53] H.-K. Tang, M. A. Marashli, and W. C. Yu, Unveiling quantum phase transitions by fidelity mapping, Phys. Rev. B **104**, 075142 (2021).

[54] M. Thesberg and E. S. Sørensen, General quantum fidelity susceptibilities for the J_1-J_2 chain, Phys. Rev. B **84**, 224435 (2011).

[55] K. Okamoto and K. Nomura, Fluid-dimer critical point in S = 1/2 antiferromagnetic Heisenberg chain with next nearest neighbor interactions, Phys. Lett. A **169**, 433 (1992).

[56] A. W. Sandvik, Ground states of a frustrated quantum spin chain with long-range interactions, Phys. Rev. Lett. **104**, 137204 (2010).

[57] S. Eggert, Numerical evidence for multiplicative logarithmic corrections from marginal operators, Phys. Rev. B **54**, R9612 (1996).

[58] H. Suwa and S. Todo, Generalized moment method for gap estimation and quantum Monte Carlo level spectroscopy, Phys. Rev. Lett. **115**, 080601 (2015).

[59] A. W. Sandvik, Computational studies of quantum spin systems, AIP Conf. Proc. **1297**, 135 (2010).

[60] H. Suwa, A. Sen, and A. W. Sandvik, Level spectroscopy in a two-dimensional quantum magnet: Linearly dispersing spinons at the deconfined quantum critical point, Phys. Rev. B **94**, 144416 (2016).

[61] J. Yang, A. W. Sandvik, and L. Wang, Quantum criticality and spin liquid phase in the Shastry-Sutherland model, Phys. Rev. B **105**, L060409 (2022).

[62] L. Wang, Y. Zhang, and A. W. Sandvik, Quantum spin liquid phase in the Shastry-Sutherland model detected by an improved level spectroscopic method, Chin. Phys. Lett. **39**, 077502 (2022).

[63] S. R. White, Density matrix formulation for quantum renormalization groups, Phys. Rev. Lett. **69**, 2863 (1992).

[64] S. R. White, Density-matrix algorithms for quantum renormalization groups, Phys. Rev. B **48**, 10345 (1993).

[65] U. Schollwöck, The density-matrix renormalization group, Rev. Mod. Phys. **77**, 259 (2005).

[66] X. Qian and M. Qin, Augmenting density matrix renormalization group with disentanglers, Chin. Phys. Lett. **40**, 057102 (2023).

[67] For systems with a width of $L \leqslant 12$, we leverage the DMRG method, preserving up to 60 000 U(1) states to ensure accurate results. In the case of a larger system of $L = 14$, we use FAMPS to perform the calculation, where we keep a maximum of 22 000 U(1) states.

[68] S. Östlund and S. Rommer, Thermodynamic limit of density matrix renormalization, Phys. Rev. Lett. **75**, 3537 (1995).

[69] F. Verstraete and J. I. Cirac, Matrix product states represent ground states faithfully, Phys. Rev. B **73**, 094423 (2006).

[70] F. Verstraete, V. Murg, and J. Cirac, Matrix product states, projected entangled pair states, and variational renormalization group methods for quantum spin systems, Adv. Phys. **57**, 143 (2008).

[71] Disentanglers are unitary matrices which transform the physical degrees of freedom of two sites. They are common building blocks in tensor networks which can reduce the local entanglement in the studied system and help to improve the accuracy of the simulation [84].

[72] T. Felser, S. Notarnicola, and S. Montangero, Efficient tensor network ansatz for high-dimensional quantum many-body problems, Phys. Rev. Lett. **126**, 170603 (2021).

[73] X. Qian and M. Qin, From tree tensor network to multiscale entanglement renormalization ansatz, Phys. Rev. B **105**, 205102 (2022).

[74] I. P. McCulloch and M. Gulácsi, The non-Abelian density matrix renormalization group algorithm, Europhys. Lett. **57**, 852 (2002).

[75] A. Weichselbaum, Non-Abelian symmetries in tensor networks: A quantum symmetry space approach, Ann. Phys. **327**, 2972 (2012).

[76] X. Li, Z. Zhou, G. Xu, R. Chi, Y. Guo, T. Liu, H. Liao, and T. Xiang, Accurate determination of low-energy eigenspectra with multitarget matrix product states, arXiv:2305.15868.

[77] T. E. Baker, A. Foley, and D. Sénéchal, Direct solution of multiple excitations in a matrix product state with block Lanczos, arXiv:2109.08181.

[78] W.-Y. Liu, J. Hasik, S.-S. Gong, D. Poilblanc, W.-Q. Chen, and Z.-C. Gu, Emergence of gapless quantum spin liquid from deconfined quantum critical point, Phys. Rev. X **12**, 031039 (2022).

[79] See Supplemental Material at http://link.aps.org/supplemental/10.1103/PhysRevB.109.L161103 for more discussion about the data used in Figs. 2 and 4, a comparison of excited energy crossing points for torus and cylinder systems, staggered magnetization [85], and the crossing point of correlation length [86,87].

[80] P. Weinberg and M. Bukov, QuSpin: a Python package for dynamics and exact diagonalization of quantum many body systems. Part II: Bosons, fermions and higher spins, SciPost Phys. **7**, 020 (2019).

[81] W.-Y. Liu, S.-S. Gong, W.-Q. Chen, and Z.-C. Gu, Emergent symmetry in quantum phase transitions: From deconfined quantum critical point to gapless quantum spin liquid, Sci. Bull. **69**, 190 (2024).

[82] C. Borgs and R. Kotecký, A rigorous theory of finite-size scaling at first-order phase transitions, J. Stat. Phys. **61**, 79 (1990).

[83] J. Haegeman, The code is developed with the TENSORKIT package at https://github.com/Jutho/TensorKit.jl.

[84] G. Vidal, Class of quantum many-body states that can be efficiently simulated, Phys. Rev. Lett. **101**, 110501 (2008).

[85] S. R. White and A. L. Chernyshev, Neél order in square and triangular lattice Heisenberg models, Phys. Rev. Lett. **99**, 127004 (2007).

[86] R. K. Kaul, Spin nematics, valence-bond solids, and spin liquids in SO(n) quantum spin models on the triangular lattice, Phys. Rev. Lett. **115**, 157202 (2015).

[87] H. Shao, W. Guo, and A. W. Sandvik, Quantum criticality with two length scales, Science **352**, 213 (2016).